frontiers | Frontiers in Materials

TYPE Original Research
PUBLISHED 06 November 2023
DOI 10.3389/fmats.2023.1297318

OPEN ACCESS

EDITED BY
In-Sung Park,
Hanyang University, Republic of Korea

REVIEWED BY
Lakshmi Narayanan Mosur Saravana Murthy,
Intel, United States
Jingbo Li,
Beijing Institute of Technology, China

*CORRESPONDENCE
Chao Ma,
machao@cdtu.edu.cn

RECEIVED 19 September 2023
ACCEPTED 23 October 2023
PUBLISHED 06 November 2023

CITATION
Ma C (2023), Modulation of optical absorption and electrical properties in Mn-Co-Ni-O-based high-entropy thin films.
Front. Mater. 10:1297318.
doi: 10.3389/fmats.2023.1297318

Modulation of optical absorption and electrical properties in Mn-Co-Ni-O-based high-entropy thin films

Chao Ma*

School of Electronic Engineering, School of Microelectronics, Chengdu Technological University, Chengdu, China

High-entropy thin films of $Mn_{0.6}Co_{0.6}Ni_{0.6}Mg_{0.6}Cu_{0.6}O_4$, $Mn_{0.6}Co_{0.6}Ni_{0.6}Mg_{0.6}Zn_{0.6}O_4$, and $Mn_{0.6}Co_{0.6}Ni_{0.6}Cu_{0.6}Zn_{0.6}O_4$ (MCNMC, MCNMZ, and MCNCZ) with equiatomic proportions were synthesized using chemical solution deposition on silicon substrates. Structural analysis confirmed a consistent face-centered cubic spinel structure, while significant differences in surface morphology were observed. Quantification of the valence states of Mn ions revealed an inverse variation in the concentrations of Mn^{4+} and Mn^{2+} ions. The heightened infrared light absorption of the MCNMC thin film was assigned to Cu-induced Jahn-Teller distortion and highly polarized Mg-O bonds. All samples exhibited negative temperature coefficient behaviors in their electrical properties. Additionally, the MCNMC thin film demonstrated the lowest resistance due to its denser microstructure, close proximity of Mn^{3+}/Mn^{4+} ion concentrations, and additional Cu^{+}/Cu^{2+} ion pairs, enhancing small polaron hopping conductivity. In contrast, the MCNMZ thin film showed moderate resistance but boasted the highest thermal constant ($B_{25/50}$) of 3768 K, attributed to its distinctive grain chain structure, facilitating carrier transport while introducing migration barriers.

KEYWORDS

high entropy, spinel, thin films, infrared absorption, electrical properties, thermistor

1 Introduction

High-entropy alloys (HEAs) have captured substantial scientific interest over the last two decades due to their exceptional mechanical properties, corrosion resistance, and thermal stability (George et al., 2019; Hu et al., 2022). Defined as alloys comprising five or more elements in nearly equal proportions and possessing a single crystal structure, HEAs have found diverse applications in nuclear fusion reactors, jet aircraft engines, and fundamental chemistry (Ren et al., 2022). Over the last decade, the concept of HEAs has expanded into various domains, including high-entropy ceramics, high-entropy thin films, high-entropy steels, and more (Sanchez et al., 2019; Wang et al., 2022). Since the introduction of rock salt-structured high-entropy ceramics in 2015, significant research interest has been directed towards medium-to high-entropy ceramic materials (Rost et al., 2015). Among them, Mn-Co-Ni-O-based high-entropy oxides have garnered significant research interest due to their distinctive magnetic, electrical, optical, and catalytic properties (Sarkar et al., 2022).

Mn-Co-Ni-O spinel oxides possess remarkable characteristics such as negative temperature coefficient (NTC) behaviors and thermal stability, rendering them highly

desirable for a wide range of applications including temperature sensors, controllers, compensators, and voltage regulators (Huang et al., 2015; Ma et al., 2016). These spinel oxides, derived from Mn_3O_4, conform to a general formula of AB_2O_4 and typically fall within the cubic space group *Fd-3m*. The crystal structure of Mn-Co-Ni-O spinel oxides is characterized by a face-centered cubic lattice, wherein oxygen ions (O^{2-}) are densely packed in a cubic close-packed arrangement, creating both tetrahedral and octahedral sites. Within this lattice, the three elements, namely, manganese (Mn), cobalt (Co), and nickel (Ni), occupy the densely stacked oxygen ion vacancies in distinct ionic valence states to maintain overall charge neutrality (Wu et al., 2010a). An outstanding feature of such materials is their sensitivity to variations in the composition of elements, resulting in changes in electrical, magnetic, optical, and thermal-sensitive properties (Zhang et al., 2014). Mn-Co-Ni-O-based high-entropy oxides, offering a wide range of elemental composition options with highly adjustable proportions, provide a significant avenue for tailoring material properties (Oses et al., 2020; Sarkar et al., 2022). For instance, Ren et al. conducted an investigation into medium-entropy oxide films of Mn-Co-Ni-O and Mn-Zn-Ni-O, revealing the profound influence of cation species and distribution on the surface morphologies and infrared (IR) optical properties (Ren et al., 2023a). Additionally, Sarkar et al. explored $(Co_{0.2}Cr_{0.2}Fe_{0.2}Mn_{0.2}Ni_{0.2})_3O_4$, employing a cross-referenced experimental approach. This investigation provided valuable insights into cation occupancy preferences, crystallographic, magnetic, and spin-electronic structures of spinel high-entropy oxides (Sarkar et al., 2022).

In response to the increasing demands of modern technology, devices employing Mn-Co-Ni-O-based materials, such as thermal elements, surge protection devices, and IR detectors, have seen significant performance requirements. Consequently, researchers have diligently sought to enhance the electrical and optical characteristics of these materials. In the context of Mn-Co-Ni-O-based materials, the concept of high entropy involves the introduction of two or more additional ions alongside the existing Mn, Co, and Ni ions. This process leads to the creation of a single-phase spinel solid solution, inevitably leading to modifications in the material's microstructure and solid solution mechanism, which profoundly impact its optical and electrical properties (Teichmann and Töpfer, 2022). Furthermore, the high entropy effect suggests that the combination of multiple elements can yield specific synergistic outcomes, occasionally resulting in unexpected effects (Wei et al., 2022). Therefore, comprehending these underlying control mechanisms can effectively optimize the performance of such high-entropy ceramic materials and expand their range of applications.

This paper investigates high-entropy thin films with the formulation $Mn_{0.6}Co_{0.6}Ni_{0.6}X_{0.6}Y_{0.6}O_4$ (X, Y = Mg, Cu, Zn) as the focal point of the study. The objective is to understand the influence of these elements on the microstructure, IR light absorption, and electron transport properties within the materials.

2 Experimental details

Thin films were fabricated with identical stoichiometric ratios of $Mn_{0.6}Co_{0.6}Ni_{0.6}Mg_{0.6}Cu_{0.6}O_4$, $Mn_{0.6}Co_{0.6}Ni_{0.6}Mg_{0.6}Zn_{0.6}O_4$, and $Mn_{0.6}Co_{0.6}Ni_{0.6}Cu_{0.6}Zn_{0.6}O_4$ through the chemical solution deposition process onto silicon substrates. These resulting samples were respectively designated as MCNMC, MCNMZ, and MCNCZ. The process involved mixing metal hydrate acetates, used as the raw materials, which were then dissolved in glacial acetic acid. The resulting solution was adjusted to a concentration of 0.2 mol/L. Subsequently, the solution underwent filtration and was spin-coated at 3,000 rpm for 30 s to generate a wet film. This film was then heated at 350°C for 5 min to eliminate residual organics and solvents. This spin-coating and heating process was repeated eight times. Finally, the film was annealed at 750°C for 1 h to promote crystallization and the formation of the desired high entropy oxide samples. Figure 1 illustrates the process of preparing high-entropy thin films.

The crystal structures of the films were determined using X-ray diffraction (XRD) analysis, conducted with a Bruker D8 Advance instrument. Scanning electron microscopy (SEM) and energy dispersive spectroscopy (EDS) were utilized, employing a Zeiss Sigma 300 instrument, to investigate the morphologies and compositions of the thin films. Elemental analyses were conducted through X-ray photoelectron spectroscopy (XPS) with Thermo Scientific K-Alpha equipment, utilizing Al Kα radiation ($h\nu$ = 1,486.8 eV). To assess the IR light absorption properties of the thin films, Fourier-transform infrared (FTIR) spectra were acquired using a Bruker TENSOR 27 instrument in attenuated total reflection (ATR) mode, with an incidence angle of 45°. Following the growth of thin films on thermally oxidized silicon substrates and the deposition of silver electrodes, electrical properties were measured using a digital multimeter (UNI-T UT805A) on a heating stage.

3 Results and discussion

3.1 Microstructure and morphology

Figure 2 shows the XRD patterns of the acquired thin film samples. These patterns exhibit distinct peaks denoted as (220), (311), (222), (400), (422), and (511), conclusively confirming that all samples possess a face-centered cubic (FCC) structure within the *Fd-3m* space group (ICDD PDF No. 00-023-1237) (Deepak et al., 2015). The lattice constants, calculated using the Bragg formula, are 8.210 Å for MCNMC, 8.230 Å for MCNMZ, and 8.229 Å for MCNCZ, respectively. Notably, the ionic radii of Mg^{2+}, Cu^{2+}, and Zn^{2+} being closely similar, the introduction of these ions into the spinel lattice does not significantly alter the lattice constant. The distribution of the Mn-Co-Ni-O oxide material can be depicted as $(Co^{2+}Mn^{2+})_T(Ni^{2+}Co^{3+}Mn^{3+}Mn^{4+})_OO^{2-}$, where the subscript *T* represents a tetrahedral site, and *O* signifies an octahedral site (Ma, 2023). Determining the precise cation distribution poses a challenge in conventional spinel oxides, further complicated in high-entropy oxides due to the presence of multiple primary cations with varying oxidation and spin states. Moreover, the low enthalpy barrier for cation anti-site mixing in spinels can lead to extreme cases of complete disorder or order (Sarkar et al., 2022). Previous studies indicate that Cu^{2+} typically occupies octahedral site, whereas Mg^{2+} and Zn^{2+} tend to occupy tetrahedral site in Mn-Co-Ni-O-based high-entropy oxides

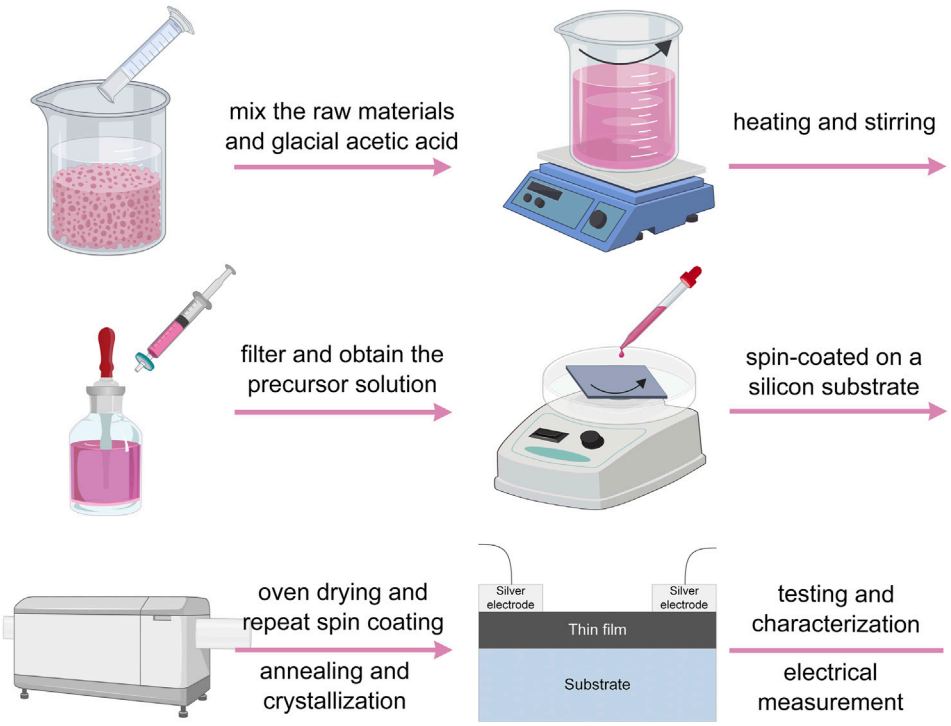

FIGURE 1
Schematic diagram of the process of preparing high-entropy thin films.

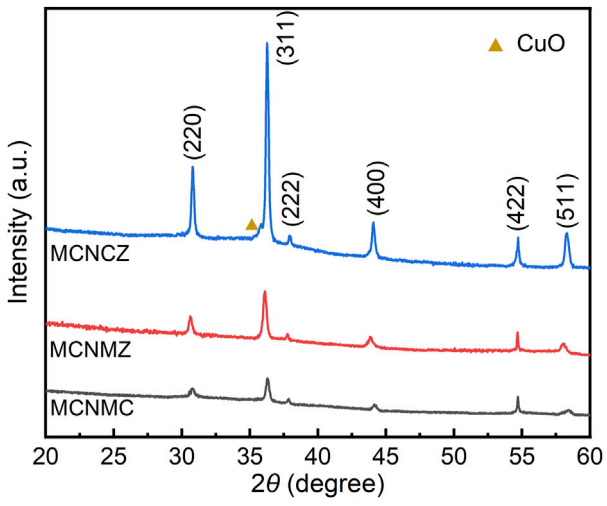

FIGURE 2
XRD patterns of the thin film samples.

(Teichmann and Töpfer, 2022; Ren et al., 2023b). However, accurate ion occupancy necessitates a combination of element-specific characterization techniques such as hard and soft X-ray near-edge absorption spectroscopy, neutron powder diffraction, and others (Sarkar et al., 2022). Regardless, the introduction of excess ions causes a shift in the concentration distribution of the original ions within the Mn-Co-Ni-O material, significantly impacting its properties, particularly its electrical characteristics (Kong et al., 2014).

In MCNCZ, the presence of a CuO impurity peak indicates a deviation from thermodynamic equilibrium within the crystal structure. The formation of CuO can be attributed to the thermodynamic instability caused by the competition between Cu ions and other cations. Specifically, in octahedral coordination, Cu ions induce the Jahn-Teller effect, leading to tetragonal distortions. Meanwhile, ions that do not induce this effect tend to maintain an octahedral environment. Consequently, there is a thermodynamic driving force for excess Cu ions to be liberated and form oxides, thus maintaining the octahedral structure (Berardan et al., 2017). In contrast, the absence of the CuO peak in MCNMC signifies the thermodynamic stability of the crystal structure. This stability can be attributed to the presence of Mg, which inhibits grain boundary migration and retards crystal growth in Mn-Co-Ni-O-based materials (Peng et al., 2012). The thermodynamic interactions between Mg ions and other cations promote the formation of cubic spinel-structured solid solutions at elevated temperatures. These conditions facilitate the integration of Cu ions into the spinel lattice, thereby inhibiting the segregation of secondary phases.

The surface morphologies of the three samples, as depicted in Figure 3, showcase pronounced variations, despite sharing identical preparation and synthesis conditions, as well as closely matched elemental compositions. While MCNMC and MCNCZ thin films exhibit similar porous surface structures, the former displays smaller particle sizes. Notably, the edges of the pores reveal a grain formation with a columnar structure, consistent with previous findings (Schwartz et al., 2004; Ma et al., 2019). During heating,

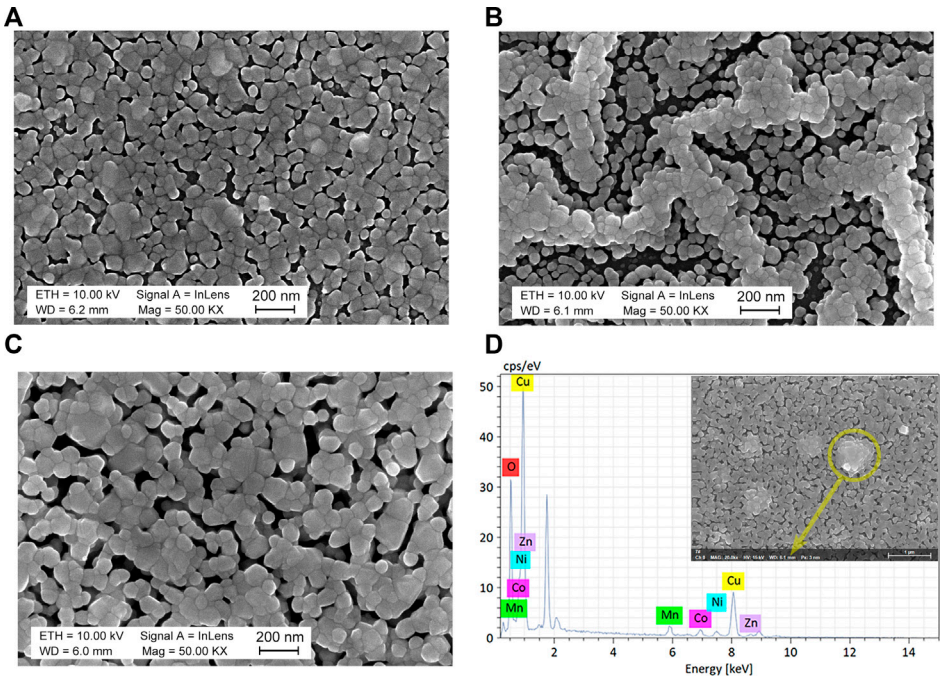

FIGURE 3
SEM images of MCNMC **(A)**, MCNMZ **(B)**, and MCNCZ **(C)** thin films. EDS point analysis of MCNCZ thin film **(D)**, along with corresponding locations in the SEM image (inset).

the substrate's surface hosts spinel nuclei from the supersaturated solution, leading to grain formation that extends to the film's surface, culminating in a columnar microstructure (Ma, 2023). In the case of the MCNMZ sample, a structure resembling chains of grains emerges. While certain grains aggregate to create denser channels, intertwining with one another, others fill in to establish a porous connected framework. The clusters of grains observed on the surface of the MCNCZ thin film are mainly identified as Cu aggregates through compositional analysis, as shown in Figure 3D, which is consistent with the XRD results. Overall, the distinct metallic elements contribute to noticeable deviations in the material's morphology, inevitably impacting the performance of Mn-Co-Ni-O-based high-entropy materials.

3.2 Chemical composition

The XPS survey spectra have revealed a diverse array of elements present within the samples. Notably, in addition to confirming the presence of Mn, Co, and Ni across all thin films, the spectra also underscore the simultaneous occurrence of Mg and Cu in the MCNMC sample, Mg and Zn in the MCNMZ sample, and Cu and Zn in the MCNCZ sample, as illustrated in Figure 4A. These findings validate the successful preparation of the high-entropy thin film samples.

The nearly symmetrical Mg 1 s peaks, located at a binding energy of 1,303.5 eV as shown in Figure 4B, confirm a 2+ oxidation state for Mg in both MCNMC and MCNMZ samples (Aksoy et al., 2012). The Zn $2p_{1/2}$ and $2p_{3/2}$ binding energies of thin films, shown in Figure 4C as peaks approximately at 1044 and 1,021 eV, respectively, can be attributed to the Zn-O bond binding energy (Aksoy et al., 2012). It is worth noting that both Zn $2p_{3/2}$ XPS peaks exhibit sharp characteristics, affirming that Zn primarily exists in the form of Zn^{2+} on the surfaces of the thin film samples (Morozov et al., 2015).

Cu 2p XPS spectra were recorded for both MCNMC and MCNCZ, as illustrated in Figure 4D. The binding energies of Cu $2p_{1/2}$ at 953 eV and Cu $2p_{3/2}$ at 933 eV can be ascribed to Cu^{2+} states (Zhao et al., 2008). Additionally, a distinct minor peak at approximately 931 eV in the MCNMC sample indicates the presence of Cu^{+} (Zhao et al., 2008). This observation signifies a more pronounced conversion from Cu^{2+} to Cu^{+} in MCNMC as compared to MCNCZ, aligning with the earlier XRD and EDS discussions that suggest an excess of Cu^{2+} in MCNCZ, thereby promoting the formation of CuO aggregates.

The resistivity of Mn-Co-Ni-O-based materials can be influenced by the small polaron hopping mechanism, where electrons transition between Mn^{3+} and Mn^{4+} ions due to phonon-electron coupling. This macroscopic charge transfer relies on the quantity of Mn^{3+}/Mn^{4+} pairs, a pivotal factor in determining the material's resistivity (Zhang et al., 2023). Consequently, comprehending the oxidation state of Mn ions and their distribution in the spinel sublattice becomes a central concern in spinel-type oxides. To address this, XPS data was peak-fitted to quantitatively analyse the diverse valence states of Mn ions near the surface of high-entropy thin films.

In Figure 5, the Mn 2p region reveals two primary peaks at approximately 653.7 eV and 642.2 eV, arising from spin–orbit

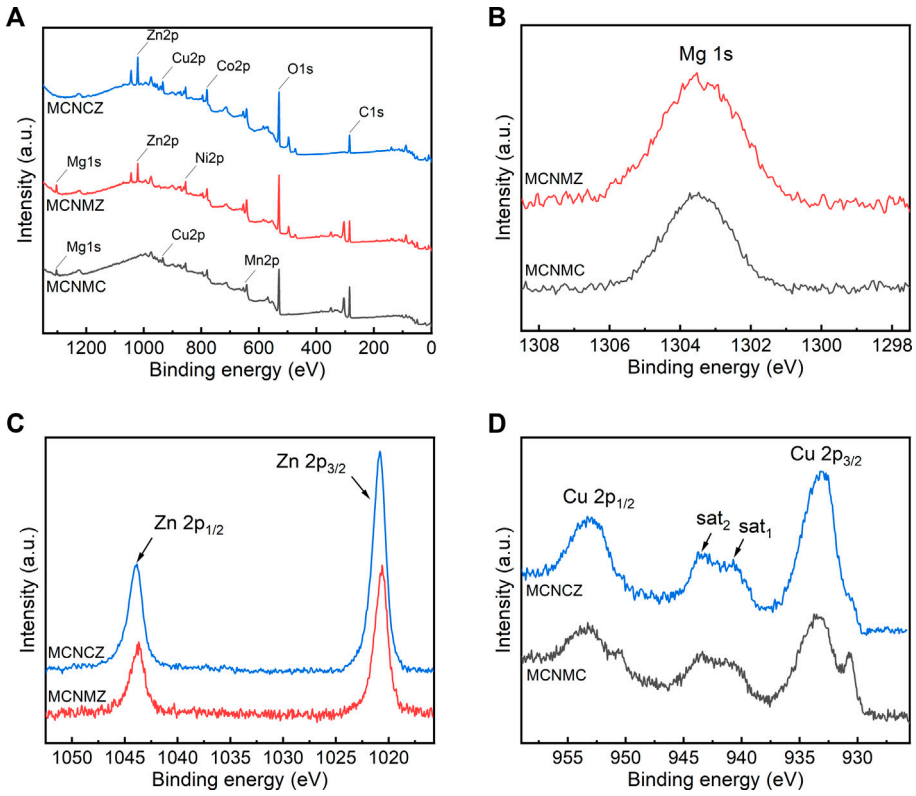

FIGURE 4
XPS survey spectra of thin films **(A)**, and XPS spectra of Mg 1 s **(B)**, Zn 2p **(C)**, and Cu 2p **(D)**. All peaks are calibrated with respect to the C 1 s peak at 284.8 eV.

coupling and identified as Mn $2p_{1/2}$ and Mn $2p_{3/2}$, respectively (Blackmore et al., 2020). Through deconvolution, the Mn $2p_{1/2}$ peak positions for all samples are observed at 655.3, 654.0 and 652.7 eV, and the Mn $2p_{3/2}$ peak positions are noted at 643.8, 642.5, and 641.2 eV, representing the Mn^{4+}, Mn^{3+}, and Mn^{2+} oxidation states, respectively. The relative concentrations of Mn^{4+}, Mn^{3+}, and Mn^{2+} on the surface of samples are calculated by determining the areas of their corresponding fitted peaks, as presented in Table 1. Significant differences in Mn ion concentrations, particularly for Mn^{4+} and Mn^{2+}, are observed among thin films containing different metal ion compositions. Among these samples, MCNMC exhibits the highest proportion of Mn ions in the higher valence state (Mn^{4+}), leading to a Mn^{4+}/Mn^{3+} ratio of 0.84, which is the closest to 1. In the MCNMC thin film, the existence of lower-valence Cu^{+} ions may cause some of the Mn^{2+} initially situated in the tetrahedral positions to transform into Mn^{4+} in the octahedral positions to maintain valence equilibrium (Marco et al., 2006). In contrast, both Mg and Zn ions consistently maintain a divalent valence state, exerting only a minor influence on the valence of the Mn ions (Ren et al., 2023b).

3.3 Infrared absorption

Improving the sensitivity of IR detectors often involves enhancing the absorption of IR light by the detector material (Hui et al., 2021). While this can be achieved by adding additional absorbing layers, there has been considerable interest in IR detectors made from self-absorbing thin-film materials due to their rapid response (Adiyan et al., 2019). In this investigation, ATR-FTIR spectroscopy is employed to elucidate the IR absorption characteristics of the thin film samples across the 7–16 μm wavelength range, as presented in Figure 6. Stringent control over sample preparation and testing conditions guarantees that the ATR-FTIR results establish a quantitative relationship encompassing the IR absorption intensities concerning the minute surfaces of the thin film samples (Ozhukil Kollath and Karan, 2016).

The IR absorption spectra indicate fundamental similarities in the IR spectra among the three samples, primarily owing to their shared spinel lattice structure, leading to consistent IR-active phonon oscillations (Paolone et al., 2000). The substantial polarizability arising from transition metals, namely, manganese, cobalt, and nickel, in combination with oxygens, results in strong coupling to external electromagnetic waves (Hou et al., 2008; Huang et al., 2015). This interaction yields a broad and robust IR spectral response, establishing Mn-Co-Ni-O as a longstanding candidate for IR detection materials. The prevalence of the Jahn-Teller effect in Mn-based spinel oxides is of great importance. This phenomenon in molecular and solid-state physics involves a molecule or polyatomic ion in an electronically degenerate state undergoing a spontaneous distortion in its molecular geometry (Reehuis et al., 2015). This distortion reduces its overall energy and eliminates the degeneracy.

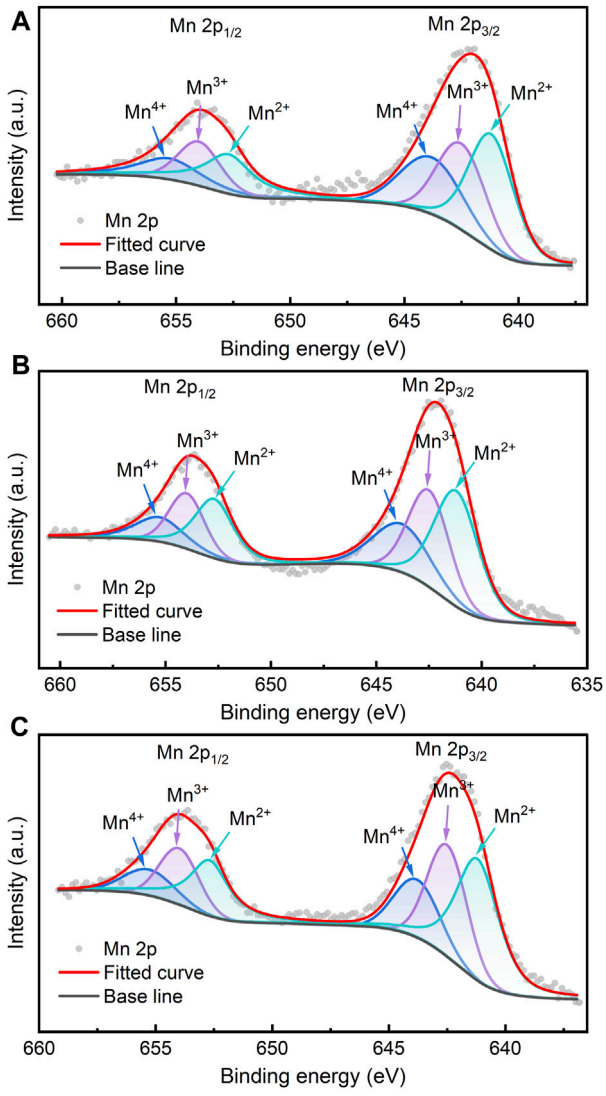

FIGURE 5
XPS spectra of Mn 2p for MCNMC **(A)**, MCNMZ **(B)**, and MCNCZ **(C)** thin film samples.

TABLE 1 Proportions of Mn cations in various valence states.

Sample	Mn^{4+} (%)	Mn^{3+} (%)	Mn^{2+} (%)	Mn^{4+}/Mn^{3+}
MCNMC	26.1	31.1	42.8	0.84
MCNMZ	23.2	32.3	44.5	0.72
MCNCZ	19.3	32.4	48.3	0.60

In the context of Mn-Co-Ni-O, this effect primarily arises from the generation of an asymmetric electron distribution within the doubly-degenerate e_g orbitals in the high-spin state of Mn^{3+} within the MnO_6 octahedron (Noh et al., 2006). Among the additional elements introduced in the high-entropy thin films, the large energy overlap between the Cu 3d energy level and the O 2p energy level allows Cu^{2+} to also induce the Jahn-Teller distortion (Jeon et al., 2021). This distortion alters the molecular

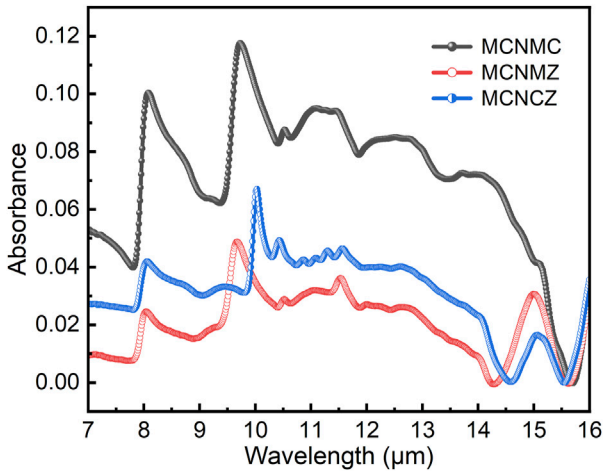

FIGURE 6
FTIR spectra of the high-entropy thin films.

structure and reduces its symmetry, increasing the dipole moment during stretching vibration and resulting in strong IR light absorption (Danielson et al., 2012).

On the other hand, an increase in the difference in electronegativity between two atoms involved in a covalent bond enhances the polarity of the bond, leading to a higher overall dipole moment of the molecule (Pritchard and Skinner, 1955). Electronegativity is often quantified via the Pauling scale. In this scale, Mg, Cu, Zn, and O have electronegativities of 1.31, 1.90, 1.65, and 3.44, respectively (Allen, 1989). The Mg-O bond, which has the greatest difference in electronegativity, will have the strongest polarity, leading to more efficient absorption of IR light during vibronic coupling. Additionally, factors such as molecular vibration frequency, energy band structure, and impurities contribute to the IR absorption of materials to some extent. Nevertheless, these findings on IR light absorption underscore the potential to significantly enhance the sensitivity of Mn-Co-Ni-O-based high-entropy thin films to IR light through a systematic design approach, providing a promising avenue for developing detectors without additional absorbing layers.

3.4 Electrical properties

Figure 7 provides a detailed overview of the electrical properties exhibited by high-entropy thin films. As illustrated in Figure 7A, the resistance of all samples exponentially decreases with increasing temperature, indicating their NTC characteristics. Figure 7B further demonstrates the nearly linear correlation between ln$R$ and $1/T$ for all samples, a relationship explained by the Arrhenius equation and its derived form (Schulze, 2008):

$$R = R_0 \exp\left(E_a/kT\right)$$
$$\ln R = \ln R_0 + E_a/kT$$

where R represents resistance, R_0 is the pre-exponential factor (independent of temperature), E_a is the activation energy, k is the

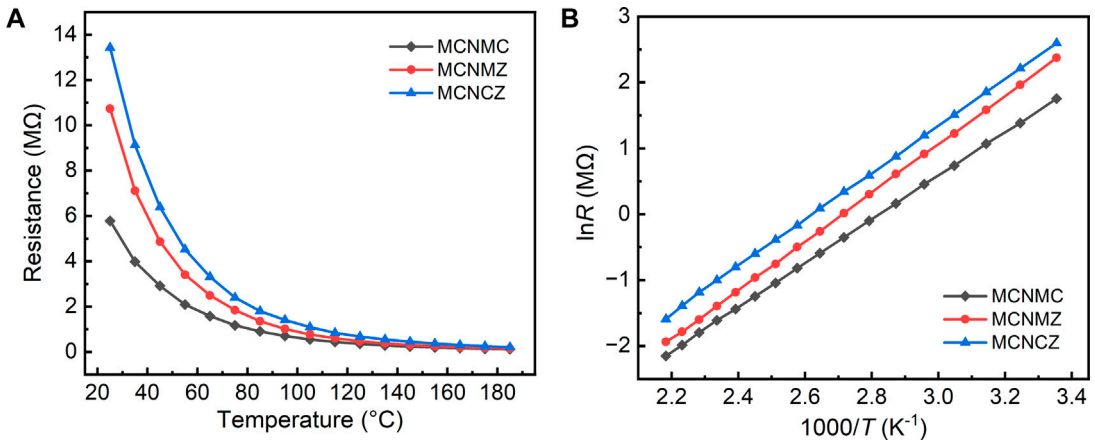

FIGURE 7
Temperature dependence of resistances in the range from 25°C to 185°C **(A)** and relationships between ln$R$ and the reciprocal of the absolute temperature **(B)** for thin film samples.

TABLE 2 Resistance (R_{25} and R_{50}), thermal constant ($B_{25/50}$), and activation energy (E_a) of high-entropy thin films.

Sample	R_{25} (MΩ)	R_{50} (MΩ)	$B_{25/50}$ (K)	E_a (eV)
MCNMC	5.78	2.44	3324	0.286
MCNMZ	10.74	4.04	3768	0.325
MCNCZ	13.43	5.36	3540	0.305

Boltzmann constant, and T signifies absolute temperature. As temperature increases, ln$R$ shows a linear decrease with $1/T$. The charge transfer mechanism in Mn-Co-Ni-O-based NTC materials has undergone extensive investigation and has been confirmed to follow the small polaron hopping model (Feteira, 2009). Specifically, Mn^{3+} ions undergo Jahn-Teller distortion within the oxygen octahedra, resulting in the creation of polarons. Due to the strong ion binding, electrons become localized into small polarons (localized electrons). The localization state of Mn^{3+} ions is closely associated with electron-phonon coupling. With the assistance of phonons, the e_g electrons of Mn^{3+} ions conduct charge transfer between the Mn^{3+} and Mn^{4+} ions, leading to a highly temperature-dependent charge transfer conduction induced by electron-phonon coupling (Dannenberg et al., 1999). The electrical performance parameters for the samples, including resistance values at 25 °C and 50 °C (R_{25} and R_{50}), thermal constant $B_{25/50}$, and the corresponding activation energy E_a, are presented in Table 2. The calculation of $B_{25/50}$ and E_a is carried out as follows:

$$B_{25/50} = \frac{\ln\left(R_{25}/R_{50}\right)}{1/T_{25} - 1/T_{50}}$$

$$E_a = B \times k$$

The significantly lower resistance of the MCNMC sample compared to the other two samples is apparent. This distinction can be observed by analyzing the surface morphology of the MCNMC thin film, which reveals smaller particles and higher densification than the other samples. This structural difference causes a reduction in the carrier transport path and time, thereby enhancing the material's conductivity (Guan et al., 2021). Secondly, as mentioned previously, Mn-Co-Ni-O-based materials adhere to the small polaron hopping model for their electrical conduction mechanism. The inclusion of Mg, Cu, and Zn ions into the high-entropy thin films leads to changes in the concentrations of Mn^{3+} and Mn^{4+} ions, with the amount of Mn^{3+}/Mn^{4+} ion pairs remaining a crucial factor affecting the electrical properties of these materials (Feteira, 2009). A rise in the number of conductive carriers taking part in the conduction process, along with an increase in hopping frequency, is directly correlated with an increase in Mn^{3+}/Mn^{4+} ion pairs (Ma et al., 2022). In Mn-based spinel materials, Cu^{+}/Cu^{2+} ion pairs have also been discovered to create small polaron hopping sites (Teichmann and Töpfer, 2022). In the case of MCNMC, the presence of Cu^{+} certainly increases the number of available hopping sites, leading to a decrease in resistance. However, the presence of CuO impurity phase in the MCNCZ sample may hinder its electrical conductivity. In the analysis of the conduction mechanism, it is imperative to consider various factors that could influence the conductivity of the material. While small polaron hopping is a plausible explanation, it is crucial to explore other potential contributors such as free carriers and oxygen vacancies. To ensure a comprehensive understanding, future studies will investigate these factors in detail.

Generally, the thermal constants of NTC thermosensitive materials exhibit a consistent relationship with changes in resistance values. This correlation stems from the correspondence between the B-value and the activation energy associated with the hopping conduction of small polarons within the materials (Ma, 2023). Larger B-values, which imply higher activation energies, imply the need to overcome a greater potential barrier during the hopping process. This, in turn, leads to an increase in resistance value (Li et al., 2023). The pores present in the MCNMZ and MCNCZ samples widen the gaps between particles, resulting in an increase in resistance. However, these pores also contribute to a higher thermal constant. The tiny pores

among the thin-film particles elongate the carriers' scattering path, increase the barriers to carrier migration, and elevate the potential barriers to be overcome (Li et al., 2020). The rise in potential barriers increases the activation energy of the material, which, in turn, affects the thermal constant. Additionally, fluctuations in ionic species and their concentration within the material can induce changes in the position, width, and occupancy of energy bands. Collectively, these changes affect the inherent potential barriers in hopping conduction, resulting in shifts in the activation energy of these high-entropy thin films (Wu et al., 2010b). Among the samples, MCNMZ exhibits a significantly high thermal constant value of 3768 K, although it does not possess the maximum resistance value. This phenomenon can be attributed to the unique grain chain structure of MCNMZ. This specific structure serves a dual role: it helps to create pathways that promote the ease of carrier transport, while at the same time introducing migration barriers between these transport channels (Ma et al., 2016).

4 Conclusion

In this study, Mn-Co-Ni-O-based high-entropy thin films with varying compositions of Mg, Cu, and Zn were prepared and characterized. Their microstructure, IR light absorption, and electrical properties were comprehensively investigated. The addition of different elements resulted in substantial changes in the microscopic morphology of the thin film materials, despite their crystal structures remaining unchanged. The concentration of Mn^{3+} ions remained nearly constant across all three samples, while the levels of Mn^{4+} and Mn^{2+} ions varied inversely. The augmented IR absorption detected in the MCNMC sample was mainly attributed to the Cu-induced Jahn-Teller distortion and highly polarized Mg-O bonds, both contributing to intensified IR absorption during vibrational coupling. The MCNMC thin film exhibited the lowest resistance owing to its denser microstructure, the proximity of Mn^{3+}/Mn^{4+} ion concentrations, and supplementary Cu^{+}/Cu^{2+} ion pairs, which enhanced small polaron hopping conductivity. In contrast, the distinctive grain chain configuration of MCNMZ attained a balance between facilitating carrier transport and establishing migration barriers, resulting in a high thermal constant. These findings provide valuable insights for tailoring the properties of high-entropy materials, particularly for their applications as sensors and detectors.

Data availability statement

The original contributions presented in the study are included in the article/Supplementary material, further inquiries can be directed to the corresponding author.

Author contributions

CM: Funding acquisition, Project administration, Resources, Supervision, Writing–original draft, Writing–review and editing.

Funding

The author(s) declare financial support was received for the research, authorship, and/or publication of this article. This research was funded by the National Natural Science Foundation of China (Grant No. 61904020).

Acknowledgments

The authors acknowledge the financial support of the National Natural Science Foundation of China (No. 61904020).

Conflict of interest

The author declares that the research was conducted in the absence of any commercial or financial relationships that could be construed as a potential conflict of interest.

Publisher's note

References

Adiyan, U., Larsen, T., Zarate, J. J., Villanueva, L. G., and Shea, H. (2019). Shape memory polymer resonators as highly sensitive uncooled infrared detectors. *Nat. Commun.* 10, 4518. doi:10.1038/s41467-019-12550-6

Aksoy, S., Caglar, Y., Ilican, S., and Caglar, M. (2012). Sol–gel derived Li–Mg co-doped ZnO films: preparation and characterization via XRD, XPS, FESEM. *J. Alloys Compd.* 512, 171–178. doi:10.1016/j.jallcom.2011.09.058

Allen, L. C. (1989). Electronegativity is the average one-electron energy of the valence-shell electrons in ground-state free atoms. *J. Am. Chem. Soc.* 111, 9003–9014. doi:10.1021/ja00207a003

Berardan, D., Meena, A. K., Franger, S., Herrero, C., and Dragoe, N. (2017). Controlled Jahn-Teller distortion in (MgCoNiCuZn)O-based high entropy oxides. *J. Alloys Compd.* 704, 693–700. doi:10.1016/j.jallcom.2017.02.070

Blackmore, R. H., Rivas, M. E., Tierney, G. F., Mohammed, K. M. H., Decarolis, D., Hayama, S., et al. (2020). The electronic structure, surface properties, and *in situ* N_2O decomposition of mechanochemically synthesised $LaMnO_3$. *Phys. Chem. Chem. Phys. PCCP* 22, 18774–18787. doi:10.1039/D0CP00793E

Danielson, J. R., Jones, A. C. L., Gosselin, J. J., Natisin, M. R., and Surko, C. M. (2012). Interplay between permanent dipole moments and polarizability in positron-molecule binding. *Phys. Rev. A* 85, 022709. doi:10.1103/PhysRevA.85.022709

Dannenberg, R., Baliga, S., Gambino, R. J., King, A. H., and Doctor, A. P. (1999). Resistivity, thermopower and the correlation to infrared active vibrations of $Mn_{1.56}Co_{0.96}Ni_{0.48}O_4$ spinel films sputtered in an oxygen partial pressure series. *J. Appl. Phys.* 86, 514–523. doi:10.1063/1.370760

Deepak, F. L., Bañobre-López, M., Carbo-Argibay, E., Cerqueira, M. F. G., Piñeiro-Redondo, Y., Rivas, J., et al. (2015). A systematic study of the structural and magnetic properties of Mn-Co-and Ni-doped colloidal magnetite nanoparticles. *J. Phys. Chem. C* 119 (21), 11947–11957. doi:10.1021/acs.jpcc.5b01575

Feteira, A. (2009). Negative temperature coefficient resistance (NTCR) ceramic thermistors: an industrial perspective. *J. Am. Ceram. Soc.* 92, 967–983. doi:10.1111/j.1551-2916.2009.02990.x

George, E. P., Raabe, D., and Ritchie, R. O. (2019). High-entropy alloys. *Nat. Rev. Mater.* 4, 515–534. doi:10.1038/s41578-019-0121-4

Guan, F., Wu, Y., Milisavljevic, I., Cheng, X., and Huang, S. (2021). Valence-induced effects on the electrical properties of $NiMn_2O_4$ ceramics with different Ni sources. *J. Am. Ceram. Soc.* 104, 5148–5156. doi:10.1111/jace.17760

Hou, Y., Huang, Z., Gao, Y., Ge, Y., Wu, J., and Chu, J. (2008). Characterization of $Mn_{1.56}Co_{0.96}Ni_{0.48}O_4$ films for infrared detection. *Appl. Phys. Lett.* 92, 202115. doi:10.1063/1.2936292

Hu, S., Fu, T., Liang, Q., Weng, S., Chen, X., Zhao, Y., et al. (2022). Formation and anisotropic mechanical behavior of stacking fault tetrahedron in Ni and CoCrFeNiMn high-entropy alloy. *Front. Mater.* 8, 813382. doi:10.3389/fmats.2021.813382

Huang, Z. M., Zhou, W., Ouyang, C., Wu, J., Zhang, F., Huang, J. G., et al. (2015). High performance of Mn-Co-Ni-O spinel nanofilms sputtered from acetate precursors. *Sci. Rep.* 5, 10899. doi:10.1038/srep10899

Hui, Y., Kang, S., Qian, Z., and Rinaldi, M. (2021). Uncooled infrared detector based on an aluminum nitride piezoelectric fishnet metasurface. *J. Microelectromechanical Syst.* 30, 165–172. doi:10.1109/JMEMS.2020.3040953

Jeon, J. E., Park, K. R., Kim, K. M., Ahn, C., Lee, J., Yu, D. Y., et al. (2021). Effect of Cu/Fe addition on the microstructures and electrical performances of Ni–Co–Mn oxides. *J. Alloys Compd.* 859, 157769. doi:10.1016/j.jallcom.2020.157769

Kong, W., Chen, L., Gao, B., Zhang, B., Zhao, P., Ji, G., et al. (2014). Fabrication and properties of $Mn_{1.56}Co_{0.96}Ni_{0.48}O_4$ free-standing ultrathin chips. *Ceram. Int.* 40, 8405–8409. doi:10.1016/j.ceramint.2014.01.049

Li, H., Thayil, I. P. L., Ma, X., Sang, X., Zhang, H., and Chang, A. (2020). Electrical properties and aging behavior of Na-doped $Mn_{1.95}Co_{0.21}Ni_{0.84}O_4$ NTC ceramics. *Ceram. Int.* 46, 24365–24370. doi:10.1016/j.ceramint.2020.06.218

Li, X., Chen, L., Hou, J., Zhao, P., Gao, B., Zhao, Q., et al. (2023). Improving the sensitivity of $LaMnO_3$ NTC films by Al ion implantation. *Vacuum* 208, 111704. doi:10.1016/j.vacuum.2022.111704

Ma, C. (2023). (1-x)$Mn_{1.56}Co_{0.96}Ni_{0.48}O_4$/x$LaMnO_3$ (0.1≤x≤0.9): a composite NTC thin film with low resistance, high sensitivity and strong light absorption. *Ceram. Int.* 49, 28442–28448. doi:10.1016/j.ceramint.2023.06.098

Ma, C., Li, N., Gao, H., and Ding, J. (2022). Effect of Ag addition on the microstructure and electrical properties of $Ni_{0.6}CoMn_{1.4}O_4$/Ag composite ceramics. *J. Alloys Compd.* 900, 163528. doi:10.1016/j.jallcom.2021.163528

Ma, C., Ren, W., and Wang, L. (2019). Thickness dependence of microstructure s and optical properties of $Mn_{1.56}Co_{0.96}Ni_{0.48}O_4$ thin films. *Optoelectron. Adv. Materials-Rapid Commun.* 13, 104–110.

Ma, C., Ren, W., Wang, L., Xu, J., Chang, A., and Bian, L. (2016). Structural, optical, and electrical properties of $(Mn_{1.56}Co_{0.96}Ni_{0.48}O_4)_{1-x}(LaMnO_3)_x$ composite thin films. *J. Eur. Ceram. Soc.* 36, 4059–4064. doi:10.1016/j.jeurceramsoc.2016.06.019

Marco, J. F., Gancedo, J. R., Nguyen Cong, H., del Canto, M., and Gautier, J. L. (2006). Characterization of $Cu_{1.4}Mn_{1.6}O_4$/PPy composite electrodes. *Solid State Ionics* 177, 1381–1388. doi:10.1016/j.ssi.2006.06.007

Morozov, I. G., Belousova, O. V., Ortega, D., Mafina, M. K., and Kuznetcov, M. V. (2015). Structural, optical, XPS and magnetic properties of Zn particles capped by ZnO nanoparticles. *J. Alloys Compd.* 633, 237–245. doi:10.1016/j.jallcom.2015.01.285

Noh, H. J., Yeo, S., Kang, J. S., Zhang, C., Cheong, S. W., Oh, S. J., et al. (2006). Jahn-Teller effect in spinel manganites probed by soft x-ray absorption spectroscopy. *Appl. Phys. Lett.* 88, 081911. doi:10.1063/1.2178474

Oses, C., Toher, C., and Curtarolo, S. (2020). High-entropy ceramics. *Nat. Rev. Mater.* 5, 295–309. doi:10.1038/s41578-019-0170-8

Ozhukil Kollath, V., and Karan, K. (2016). New molecular scale insights into the alpha-transition of Nafion® thin films from variable temperature ATR-FTIR spectroscopy. *Phys. Chem. Chem. Phys. PCCP* 18, 26144–26150. doi:10.1039/C6CP04457C

Paolone, A., Roy, P., Pimenov, A., Loidl, A., and Shapiro, A. Y. (2000). Infrared phonon spectrum of pure and doped $LaMnO_3$. *Phys. Rev. B* 61, 11255–11258. doi:10.1103/PhysRevB.61.11255

Peng, C., Zhang, H., Chang, A., Guan, F., Zhang, B., and Zhao, P. (2012). Effect of Mg substitution on microstructure and electrical properties of $Mn_{1.25}Ni_{0.75}Co_{1.0-x}M_xO_4$ (0≤x≤ 1) NTC ceramics. *J. Mater. Sci. Mater. Electron.* 23, 851–857. doi:10.1007/s10854-011-0505-8

Pritchard, H. O., and Skinner, H. A. (1955). The concept of electronegativity. *Chem. Rev.* 55, 745–786. doi:10.1021/cr50004a005

Reehuis, M., Tovar, M., Többens, D. M., Pattison, P., Hoser, A., and Lake, B. (2015). Competing Jahn-Teller distortions and ferrimagnetic ordering in the geometrically frustrated system $Ni_{1-x}Cu_xCr_2O_4$. *Phys. Rev. B* 91, 024407. doi:10.1103/PhysRevB.91.024407

Ren, J., Zhang, Y., Zhao, D., Chen, Y., Guan, S., Liu, Y., et al. (2022). Strong yet ductile nanolamellar high-entropy alloys by additive manufacturing. *Nature* 608, 62–68. doi:10.1038/s41586-022-04914-8

Ren, W., Ding, T., Wang, W. L., Zhang, Y. X., Li, Y., Lu, Y. T., et al. (2023b). Microstructure and cation distribution of $Mn_{2-x}Al_xZn_{0.2}Ni_{0.6}Mg_{0.2}O_4$ high entropy oxide films. *J. Mater. Sci. Mater. Electron.* 34, 655. doi:10.1007/s10854-023-10082-w

Ren, W., Zhang, Y. X., Wang, W. L., Ding, T., Zhou, Q., Wu, H. B., et al. (2023a). Structural and optical properties of Mn–Co–Ni–O and Mn–Zn–Ni–O medium-entropy oxide films. *J. Mater. Sci. Mater. Electron.* 34, 386. doi:10.1007/s10854-022-09795-1

Rost, C. M., Sachet, E., Borman, T., Moballegh, A., Dickey, E. C., Hou, D., et al. (2015). Entropy-stabilized oxides. *Nat. Commun.* 6, 8485. doi:10.1038/ncomms9485

Sanchez, J. M., Vicario, I., Albizuri, J., Guraya, T., and Garcia, J. C. (2019). Phase prediction, microstructure and high hardness of novel light-weight high entropy alloys. *J. Mater. Res. Technol.* 8, 795–803. doi:10.1016/j.jmrt.2018.06.010

Sarkar, A., Eggert, B., Witte, R., Lill, J., Velasco, L., Wang, Q., et al. (2022). Comprehensive investigation of crystallographic, spin-electronic and magnetic structure of $(Co_{0.2}Cr_{0.2}Fe_{0.2}Mn_{0.2}Ni_{0.2})_3O_4$: unraveling the suppression of configuration entropy in high entropy oxides. *Acta Mater.* 226, 117581. doi:10.1016/j.actamat.2021.117581

Schulze, H. M. (2008). *Synthesis and characterization of nickel manganite thin films for application in uncooled microbolometers*. M.S. Thesis. University Park, PA: The Pennsylvania State University.

Schwartz, R. W., Schneller, T., and Waser, R. (2004). Chemical solution deposition of electronic oxide films. *Comptes Rendus Chim.* 7, 433–461. doi:10.1016/j.crci.2004.01.007

Teichmann, C., and Töpfer, J. (2022). Sintering and electrical properties of Cu-substituted Zn-Co-Ni-Mn spinel ceramics for NTC thermistors thick films. *J. Eur. Ceram. Soc.* 42, 2261–2267. doi:10.1016/j.jeurceramsoc.2021.12.078

Wang, B., Yao, J., Zhao, P., Wang, J., and Chang, A. (2022). A comparative study of different oxidation states of raw materials on the properties of a novel medium-entropy $Co_{2.77}Mn_{1.71}Fe_{1.10}Zn_{0.42}O_8$ thermistor materials. *Mater. Chem. Phys.* 284, 126018. doi:10.1016/j.matchemphys.2022.126018

Wei, J. H., Ren, W., Lu, H., Yao, G. G., Zhu, Y., Zhao, D. X., et al. (2022). Synthesis of medium entropy $Mn_{1.56}Co_{0.96}Ni_{0.48}O_4$ films by solid-state reaction. *J. Solid State Chem.* 306, 122742. doi:10.1016/j.jssc.2021.122742

Wu, J., Huang, Z., Hou, Y., Gao, Y., and Chu, J. (2010a). Structural, electrical, and magnetic properties of $Mn_{2.52-x}Co_xNi_{0.48}O_4$ films. *J. Appl. Phys.* 107, 053716. doi:10.1063/1.3309780

Wu, J., Huang, Z., Hou, Y., Gao, Y., and Chu, J. (2010b). Variation in hopping conduction across the magnetic transition in spinel $Mn_{1.56}Co_{0.96}Ni_{0.48}O_4$ films. *Appl. Phys. Lett.* 96, 082103. doi:10.1063/1.3318459

Zhang, F., Ju, J., Huo, D., Wu, L., Lei, Y., and Zhang, Y. (2023). Photoelectric and photocatalytic properties of long-time annealing Mn–Co–Ni–O thin film. *J. Mater. Sci. Mater. Electron.* 34, 523. doi:10.1007/s10854-023-09934-2

Zhang, H., Chang, A., Guan, F., Zhao, L., Zhao, Q., Yao, J., et al. (2014). The optimal synthesis condition by sol–gel method and electrical properties of $Mn_{1.5-x}Co_{1.5}Ni_xO_4$ ceramics. *Ceram. Int.* 40, 7865–7872. doi:10.1016/j.ceramint.2013.12.133

Zhao, C., Wang, B., Yang, P., Winnubst, L., and Chen, C. (2008). Effects of Cu and Zn co-doping on the electrical properties of $Ni_{0.5}Mn_{2.5}O_4$ NTC ceramics. *J. Eur. Ceram. Soc.* 28, 35–40. doi:10.1016/j.jeurceramsoc.2007.06.007